

Diagnostics of non-thermal processes in chromospheric flares

IV. Limb flare spectra for an atmosphere bombarded by an electron beam

C. Fang^{1,2}, J.-C. Hénoux², and M.D. Ding¹

¹ Nanjing University, Department of Astronomy, Nanjing, P.R. China

² Observatoire de Paris, DASOP-UMR8645 (CNRS), 92195 Meudon Cedex, France

Received 8 June 1999 / Accepted 30 May 2000

Abstract. $H\alpha$, $Ly\alpha$, $Ly\beta$, CaII K and $\lambda 8542 \text{ \AA}$ line profiles have been computed for limb flares with height distributions of temperatures as given by the semi-empirical models F_1 and F_2 , by including the non-thermal collisional excitation and ionization of hydrogen and of ionized calcium that results from electron bombardment. In agreement with observations, the computed profiles of the hydrogen lines are very broad, especially at the height where the source function reaches its maximum. Non-thermal effects are less pronounced for CaII lines.

Key words: line: profiles – radiation mechanisms: non-thermal–Sun: flares

1. Introduction

It is well known that in the impulsive phase of solar flares, the Balmer lines are very broad, while the metal lines remain extremely narrow (Švestka 1976). However, in limb flare spectra the already rather broad profiles of the hydrogen lines still broaden (e.g. Graeter & Kucera 1992; Ding et al. 1999). Moreover, metal lines lose their sharp and narrow characters and, in some cases, their width becomes comparable to that of the high Balmer lines (Švestka 1976). In this case, if one compares the widths of lines from two elements of very different atomic weights, unacceptable high values of the temperature and of the micro-turbulence velocity are obtained (e.g. Jefferies & Orral 1961; Švestka 1965). Recently an unusually broad profile of the HeI $\lambda 10830$ line was observed by You et al. (1998) in a large limb flare. This behaviour could be interpreted neither by a Doppler broadening mechanism, nor by a pure Stark effect, that would imply an unacceptable high electron density (You & Oertel 1992). Here we give a new example (Ding et al. 1999). Fig. 1 shows an $H\alpha$ image of a limb flare that occurred on 11 November, 1998. The flare is a small one (SF/C3.2) that was observed with an imaging spectrograph at the solar tower of Nanjing University (Huang et al. 1995). Fig. 2 gives the line profiles of the $H\alpha$ and CaII 8542 lines, which were observed simultaneously before the $H\alpha$ maximum. It can be seen that, even for this small flare, the line profiles are extremely broad.

Send offprint requests to: C. Fang

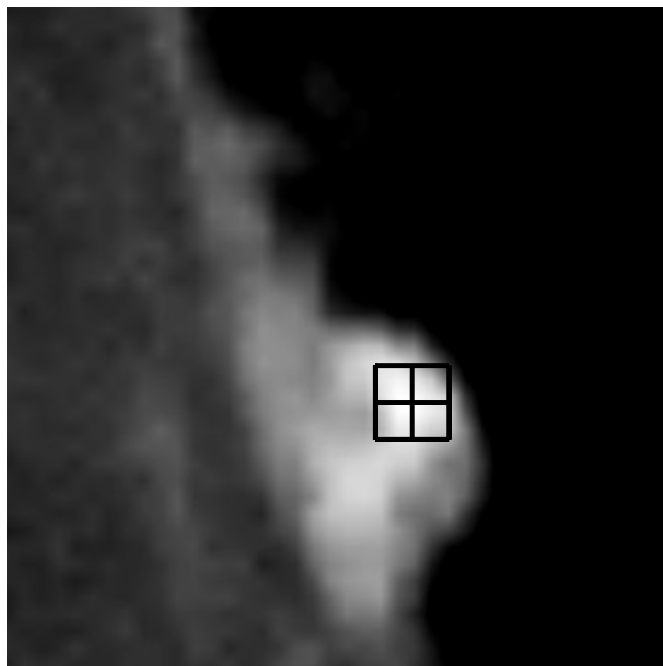


Fig. 1. Monochromatic image at $H\alpha$ line center of a limb flare at 02:14:38 UT. The field of view is $60'' \times 60''$. North is up, east is to the left

The widths at half-peak intensity of the $H\alpha$ and CaII 8542 lines are about 6 \AA and 1.6 \AA , respectively. By using these values and assuming a Doppler broadening, a temperature as high as $1.6 \times 10^6 \text{ K}$ and a micro-turbulence velocity of 21 km s^{-1} would be obtained. Obviously, this is not reasonable. Thus, how the extreme broadening of the line profiles observed in limb flare spectra can be explained is an interesting problem worth studying in detail.

By considering the effect of non-thermal collisional excitation and ionization of hydrogen and CaII, by an electron beam, we have shown that the hydrogen lines in the spectra of disk flares are greatly strengthened and broadened, while the resulting broadening is weaker for the CaII K line (Fang et al. 1993; Hénoux et al. 1995, hereafter referred to as Paper I and II, respectively).

It is worth computing for limb flares the hydrogen and CaII line spectra, including the effect of non-thermal collisional excitation and ionization, in order to learn how these processes contribute to the line broadening observed in limb flares spectra. We follow the theory and the method given in Papers I and II, and show non-thermal line profiles, computed for a limb flare atmosphere bombarded by an electron beam. The methodology is given in Sect. 2. The main results are shown in Sect. 3 and followed by a discussion and conclusion in Sect. 4.

2. Methodology

A four-levels plus continuum atomic model of hydrogen was used. Following the theory given in Paper I and II, to a good approximation, for an electron beam bombardment, the non-thermal collisional excitation and ionization rates of hydrogen from its ground level can be obtained as

$$\begin{aligned} C_{12}^B &\simeq 2.94 \cdot 10^{10} \frac{1}{n_1} \frac{dE^H}{dt}, & \text{and} & & C_{13}^B &\simeq 5.35 \cdot 10^9 \frac{1}{n_1} \frac{dE^H}{dt}, \\ C_{14}^B &\simeq 1.91 \cdot 10^9 \frac{1}{n_1} \frac{dE^H}{dt}, & \text{and} & & C_{1c}^B &\simeq 1.73 \cdot 10^{10} \frac{1}{n_1} \frac{dE^H}{dt}, \end{aligned} \quad (1)$$

The non-thermal collisional excitation and ionization rates of CaII, as given in Paper I, can be expressed as

$$\begin{aligned} C_{14}^B(\text{CaII}) &\simeq 2.38 \cdot 10^{10} \frac{1}{n_1} \frac{dE^H}{dt}, \\ C_{15}^B(\text{CaII}) &\simeq 4.25 \cdot 10^{10} \frac{1}{n_1} \frac{dE^H}{dt}, \\ C_{1c}^B(\text{CaII}) &\simeq 4.69 \cdot 10^{10} \frac{1}{n_1} \frac{dE^H}{dt}, \end{aligned} \quad (2)$$

where n_1 is the ground level population. dE^H/dt is the rate of energy deposit due to the excitation and ionization of hydrogen by an electron beam. The excitation and ionization from the higher levels are negligible. Neglecting return current effects in a dense atmosphere, the energy deposit rate is given by (Emslie 1978; Chambe & Hénoux 1979)

$$\begin{aligned} \frac{dE^H}{dt} = & \\ \frac{1}{2}(1-x)n_H\Lambda' \frac{K\mathcal{F}_1}{E_1^2} \left(\frac{N}{N_1}\right)^{-\frac{\delta}{2}} (\delta-2) \int_0^{u_1} \frac{u^{\frac{\delta}{2}-1} du}{(1-u)^{\frac{2+\beta}{4+\beta}}}, \end{aligned} \quad (3)$$

where x is the ionization degree. The particle flux is supposed to be proportional to $E^{-\delta}$, with a low cut-off energy E_1 . \mathcal{F}_1 is the total energy input flux above E_1 . The meaning of other physical quantities can be found in the relevant references.

In most empirical flare models, the chromospheric flare is located at heights lower than the top of the chromosphere (~ 2000 km) in the quiet-Sun model VAL-C given by Vernazza et al. (1981). If this property was valid for all flares, one would actually not see any structure above the solar limb and no any limb flares. This is not the case, since limb flares are observed.

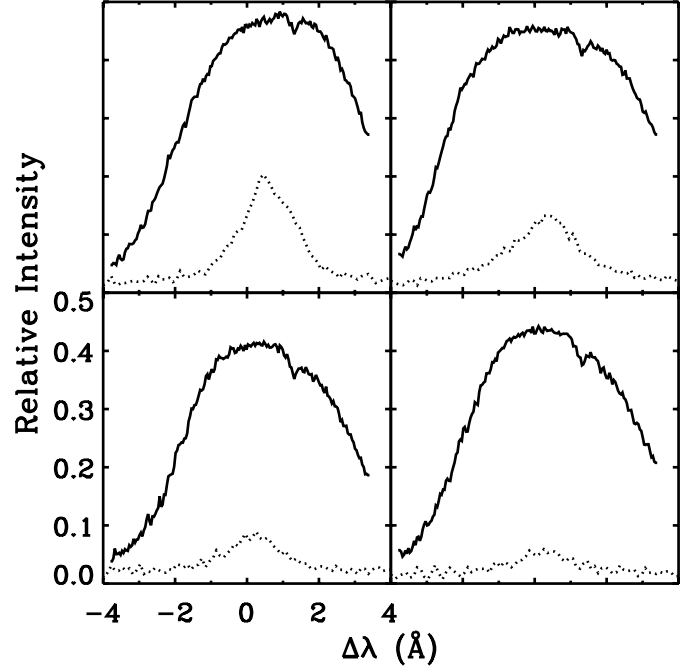


Fig. 2. Line profiles of the H α (solid lines) and Ca II λ 8542 (dashed lines) lines at 02:14:18 UT. Each panel has a one to one correspondence to each small square shown in Fig. 1

Thus, in order to compute the profile of chromospheric lines in limb flares, we need a specific empirical model. Unfortunately no such model exists. Therefore, in this paper, the temperature distribution in the flaring atmosphere has been represented by the semi-empirical flare models F₁ and F₂ given by Machado et al. (1980). In these models, a plan parallel atmosphere has been used. Indeed we cannot, in such conditions, study in a satisfactory way the height dependence of the line profiles. However, this approach allows us to explore the role of the non-thermal effects of particle beams in the line profiles of limb flares. The heights given in the figures may not be correct; however, they correspond to specific values of density and temperature. The comparison between observed and computed profiles could allow us to estimate the height variation of the density and temperature for a given limb flare. We shall not go so far as to limit ourselves to the demonstration that additional effects, due to non-thermal processes are required in order to explain the significant width of the observed line profiles.

The numerical code we used is similar to the one presented in Papers I and II. That is, the non-thermal rates have been included in the statistical equilibrium equations; the statistical equilibrium equations and the transfer equations for hydrogen and CaII, coupled with the hydrostatic equilibrium and the particle conservation equations, have been solved iteratively. One hundred frequency-points have been used for each line concerned. Five broadening mechanisms, i.e. Doppler broadening, radiative damping, Van de Waals forces, linear and quadratic Stark effects, have been included in the calculation of the line profiles. The assumption of complete frequency redistribution was adopted for simplicity. This does not have a significant influ-

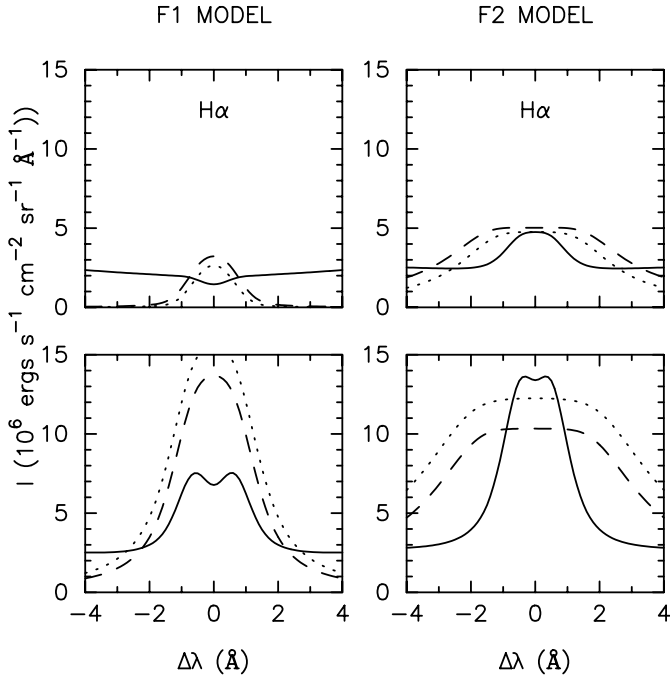


Fig. 3. $H\alpha$ line profiles for the models F_1 (left panel) and F_2 (right panel), with (lower panel) and without (upper panel) non-thermal effects included. Line profiles for a flare at the center of the solar disk (full line) and at the limb at heights of 1300 km (dashed line) and 1040 km (dotted line), for the F_1 model, and 1180 km (dashed line) and 1140 km (dotted line), for the F_2 model, are shown respectively. A Gaussian macroturbulence velocity of 25 km s^{-1} has been adopted to convolve the line profiles

ence on the line wing intensities, where the non-thermal effects are the most pronounced. Using the flare atmospheric models F_1 and F_2 , we computed the source function S_λ and the opacity χ_λ at different heights of the atmosphere. Assuming that, for a limb flare, the horizontal distributions of the source function are constant for a given height, we can compute the line profiles at different heights by using

$$I_\lambda = S_\lambda(1 - e^{-\tau_\lambda}), \quad (4)$$

where $\tau_\lambda = \chi_\lambda D$. D is the thickness of the flare along the line-of-sight and χ_λ is the absorption coefficient per unit length. We take $D = 3000 \text{ km}$ as typical for all the models. The value of D does not influence greatly the final results. The calculations have been made for an electron beam with an initial total energy flux $\mathcal{F}_1 = 5 \cdot 10^{11} \text{ ergs cm}^{-2} \text{ s}^{-1}$ and with a power index δ equal to 4, which are typical values for flares. The low cut-off energy E_1 was chosen to be 20 keV; the origin of the electron beam was taken at the top of the chromosphere, where the column mass $M_0 = 0$. In the upper and middle chromosphere, where the lines are formed, the mean hydrogen ionization degree $\bar{x} \simeq 0.5$ and $\Lambda' \simeq 9$ for an electron beam with an energy of several tens of keV. So $\bar{\beta} \simeq 2$ and $\bar{\gamma} \simeq 15$ were adopted.

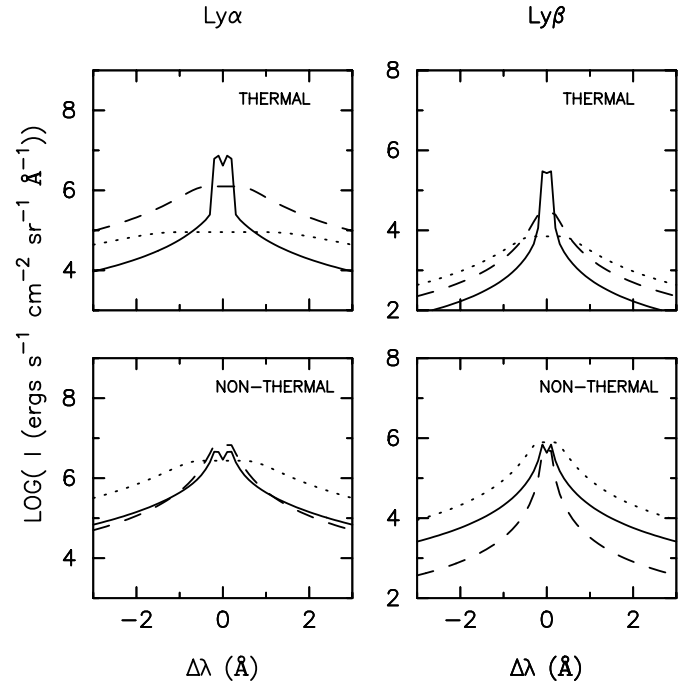


Fig. 4. $Ly\alpha$ and $Ly\beta$ line profiles for the model F_1 . “Thermal” line profiles are shown in the upper panel, while “non-thermal” profiles are presented in the lower panel. The line profiles at the center of the solar disk are drawn in full lines, while that for a limb flare at heights of 1530 km and 1300 km are shown with dashed and dotted lines, respectively

3. Numerical results

Fig. 3 shows the $H\alpha$ line profiles for models F_1 and F_2 , with (lower panel) and without (upper panel) non-thermal hydrogen collisional excitation and ionization included. Fig. 4 shows the $Ly\alpha$ and $Ly\beta$ line profiles for the model F_1 . The profiles obtained by adding or not the collisional excitation and ionization rates to the thermal ones are shown respectively in the lower and upper panels. It can be seen that non-thermal processes greatly influence the intensity and the broadening of the hydrogen line profiles of limb flares. This effect is especially obvious in $H\alpha$ line, while the $Ly\alpha$ and $Ly\beta$ line profiles are relatively less affected, though in the non-thermal case the intensities of both lines are increased by more than one order of magnitude and they are broader than in the thermal case.

Fig. 5 shows the CaII K and IR $\lambda 8542 \text{ \AA}$ line profiles for the model F_2 , with (lower panel) and without (upper panel) non-thermal effects included. It can be seen that the CaII lines of a flare at the limb are broader than at the center of the solar disk, though the effect of non-thermal broadening for the CaII lines is less obvious than for the $H\alpha$ line. This is not surprising, because non-thermal effects for the CaII lines are weaker than for the hydrogen lines, as was indicated in our Paper I.

To clearly understand the non-thermal broadening effect, the column mass distributions of the source function and of the optical depth at the center and at $+1.5 \text{ \AA}$ of the $H\alpha$ line for models F_1 and F_2 , respectively, are plotted in Fig. 6. The figure shows that the source function in the non-thermal case is

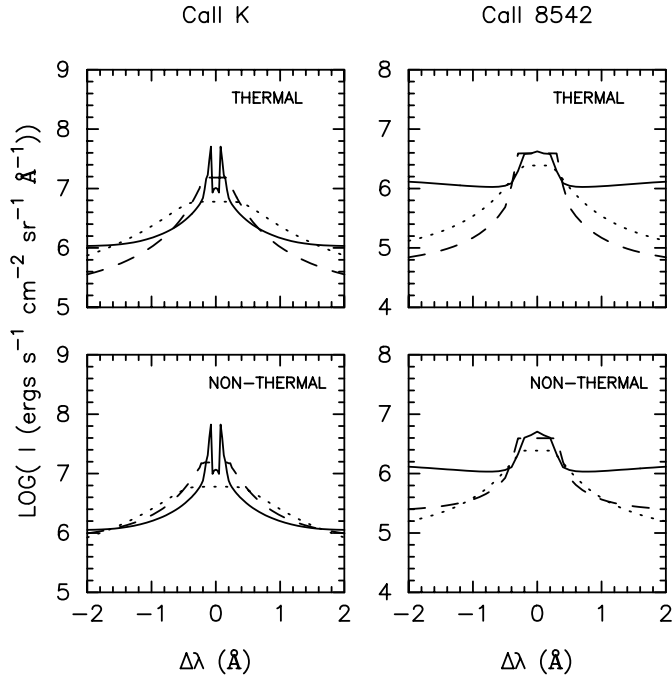


Fig. 5. CaII K and $\lambda 8542 \text{ \AA}$ line profiles for the model F₂, with (lower panel) and without (upper panel) non-thermal effects included. The full lines show the line profiles at the center of the solar disk, while the dashed and dotted lines give the line profiles for a limb flare at heights of 1140 km and 800 km, respectively

much larger than that in the thermal case, as already indicated in Paper II. However, its value changes with height: generally it decreases with height, except for the F₁ model in the non-thermal case, where the source function attains its maximum around $M=0.01$. At the line center, except for the upper layers of flaring atmosphere, the optical depth $\tau_\lambda > 1$; while at the line wings, $\tau_\lambda < 1$ through all the layers. When a flare is observed on the solar disk, the line wing intensity is some weighted average of the source function through all the atmosphere. For limb flares, if the height of observation just corresponds to the place where the source function attains its maximum, then the intensities at line wings are greatly increased; so that the width of the line profile is much enlarged. In the F₁ model, this happens around $M=0.01$, where M is the column mass, corresponding to a height of around 750-850 km; while in the F₂ model, it is in the very upper layers of the flaring atmosphere. This is illustrated in Figs. 3 and 4. As concerns the CaII lines, as shown in Fig. 7, the situation is similar to the one for hydrogen lines. However, there is no obvious difference between the thermal and the non-thermal source functions, except at the very upper layers of the F₁ model; so the line widths of limb flares are similar for both cases, though in the non-thermal case, the lines are somewhat broader than those in the thermal case.

4. Discussion and conclusion

Our results show that in a flare, when an electron beam bombards the atmosphere, the lines, when observing the flare spectra

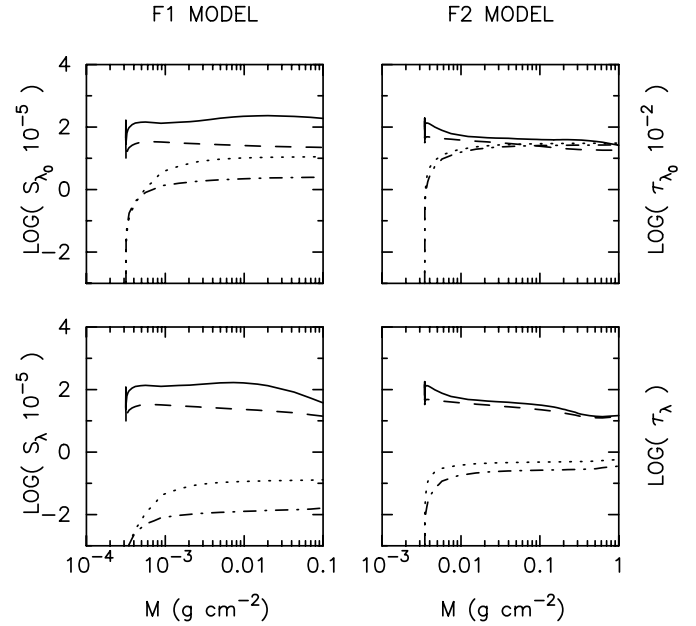


Fig. 6. Column mass distributions of the source function (full and dashed lines for the non-thermal and thermal case respectively) and of the optical depth (dotted and dotted-dashed lines for the non-thermal and thermal case respectively) at the center (upper panel) and at $+1.5 \text{ \AA}$ (lower panel) of the H α line for the models F₁ (left panel) and F₂ (right panel), respectively

on the limb, should be greatly broadened. This effect is especially pronounced for the hydrogen lines, and is mainly due to the enhancement of the source function through non-thermal collisional excitation and ionization of hydrogen and CaII by electron beam bombardment.

In our calculations, at a given height, the source function is assumed to be constant along the line of sight. This is presumably true for the impulsive phase of flares, when the particle beam bombards the chromosphere. Because at this phase, the input energy comes mainly from magnetic reconnection and is much larger than the radiative cooling, which has a longer time scale, of the order of tens of minutes (e.g. Gan & Fang 1990). Indeed, due to the radiation escape at the boundaries of a structure above the limb, such as a prominence, the H α source function may decrease toward the surface of the structure, as indicated by Gouttebroze et al. (1993). However, even if the source function decreases toward the surface, which may reduce the intensity at the line center, the half-width of the line would still remain high, because the optical depth at the line wings is less than unit, so their intensities result from the integration of the source function through the whole flare structure and are therefore not significantly affected by its decrease at the structure boundaries. Thus, the assumption of constant source function is probably acceptable.

Some authors suggested that large scale non-Maxwellian motions could be responsible for the line broadening observed in limb flares (e.g. Jefferies & Orrall 1961; Švestka 1965, 1976; You et al. 1998). This is probably partially true, but why only limb flares would have such large non-Maxwellian motions is still not

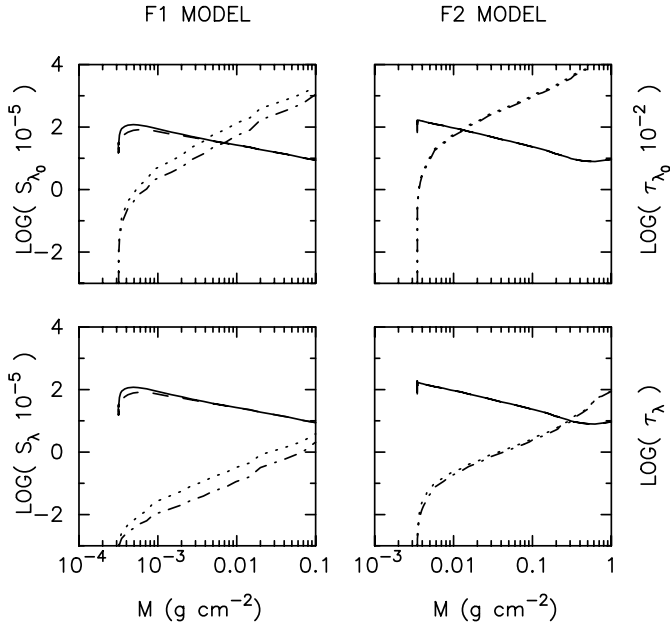


Fig. 7. Column mass distributions of the source function (full and dashed lines for the non-thermal and thermal case respectively) and of the optical depth (dotted and dotted-dashed lines for the non-thermal and thermal case respectively) at the center (upper panel) and at $+1.0\text{\AA}$ (lower panel) of the CaII K line for models F₁ (left panel) and F₂ (right panel), respectively

clear. One probable explanation is that, indeed, one can only see the upper part of the atmosphere in flares observed above the limb, so if the non-Maxwellian and/or the micro-turbulence velocity increases with height, then they could contribute to the line broadening in limb flare spectra and without having any significant contribution to the broadening of the profiles in observations of flares on the disk. However, according to the analysis in Sect. 3, very broad line profiles, especially for hydrogen lines, will be observed in limb flares when non-thermal effects are taken into account, even if the non-Maxwellian and/or the micro-turbulence velocity do not increase with height. Thus, non-thermal collisional excitation and ionization should be one of the most significant line broadening sources in limb flare spectra.

In summary:

1. The great broadening of the profiles of hydrogen lines that is observed in limb flare spectra can be at least partly explained by the non-thermal excitation and ionization of hydrogen by electron bombardment of the flaring atmosphere. This effect is less pronounced for CaII lines.

2. The non-thermal broadening of the line profiles is especially pronounced at the height where the hydrogen line source function attains its maximum. As shown in Fig. 3 for the F₁ model, this is not necessary in the upper boundary layers at chromospheric temperature during flares. This can probably provide a valuable diagnostic tool to distinguish the effect of non-Maxwellian motions increasing with height from that of non-thermal collisional excitation and ionization caused by particle beams.

Acknowledgements. C. Fang would like to express his sincere gratitude to the Paris Observatory for supporting his stay and for kind hospitality. Many thanks are also due to Dr. Heinzel for his valuable comments and help. This work was partly supported by a key project from the Ministry of Science and Technology, by funds from the National Natural Science Foundation (No. 49990451) and from the Ministry of Education of P.R. China.

References

- Chambe G., Hénoux J.-C., 1979, A&A 80, 123
 Ding M.D., Fang C., Yin S.Y., Chen P.F., 1999, A&A 348, L29
 Emslie A.G., 1978, ApJ 224, 241
 Fang C., Hénoux J.-C., Gan W.Q., 1993, A&A 274, 917 (Paper I)
 Gan W.Q., Fang C., 1990, ApJ 358, 328
 Graeter M., Kucera T.A., 1992, Solar Phys. 141, 91
 Gouttebroze P., Heinzel P., Vial J.C., 1993, A&AS 99, 513
 Hénoux J.-C., Fang C., Gan W.Q., 1995, A&A 297, 574 (Paper II)
 Huang Y.R., Fang C., Ding M.D., et al., 1995, Solar Phys. 159, 127
 Jefferies J.T., Orrall F.Q., 1961, ApJ 133, 946; 963
 Machado M.E., Avrett E.H., Vernazza J.E., Noyes R.W., 1980, ApJ 242, 336
 Švestka Z., 1965, Adv. Astron. Astrophys. 3, 119
 Švestka Z., 1976, In: Solar Flares. D. Reidel Publ. Co., p. 55
 You J., Oertel G.K., 1992, ApJ 389, L33
 You J., Wang C., Fan Z., Li H., 1998, Solar Phys. 182, 431
 Vernazza J.E., Avrett E.H., Loeser R., 1981, ApJS 45, 635